Journal of Instrumentation

You may also like

- Linear analysis of single-shot dual-energy computed tomography with a multilayer detector
S. Ha, J. Kim, J. Yun et al.
- The SMILE Soft X-ray Imager (SXI) CCD design and development
M.R. Soman, D.J. Hall, A.D. Holland et al.
- Time-of-flight measurements at the Super-FRS
C Nociforo

The antares neutrino detector instrumentation

To cite this article: H Yepes-Ramírez 2012 *JINST* **7** C01022

View the article online for updates and enhancements.

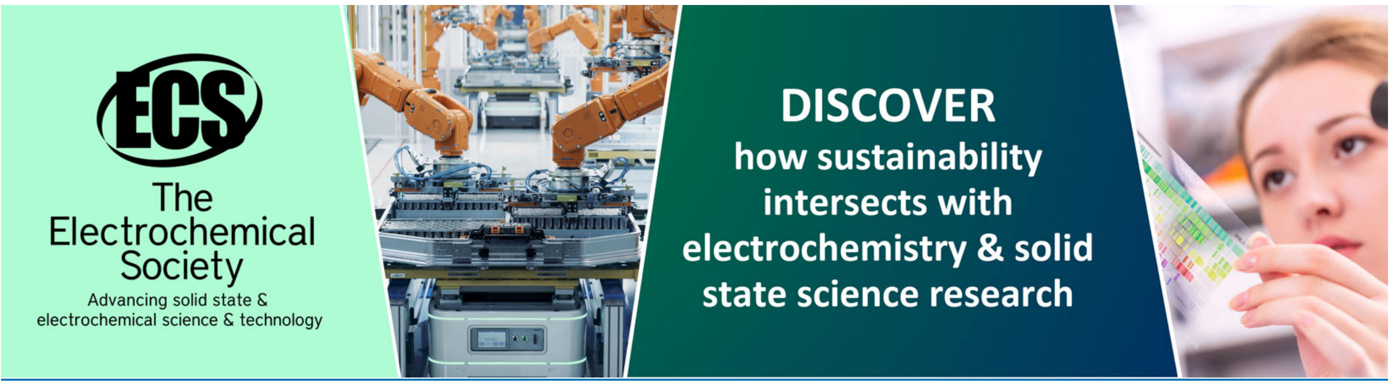

This content was downloaded from IP address 3.147.67.166 on 06/05/2024 at 07:52

*J*inst

PUBLISHED BY IOP PUBLISHING FOR SISSA

RECEIVED: *October 31, 2011*
REVISED: *December 9, 2011*
ACCEPTED: *December 9, 2011*
PUBLISHED: *January 5, 2012*

TOPICAL WORKSHOP ON ELECTRONICS FOR PARTICLE PHYSICS 2011,
26–30 SEPTEMBER 2011,
VIENNA, AUSTRIA

2012 JINST 7 C01022

The antares neutrino detector instrumentation

H. Yepes-Ramírez

Instituto de Física Corpuscular (IFIC),
Edificios de Investigación de Paterna, CSIC - Universitat de València,
Apdo. de Correos 22085, E-46071 Valencia, Spain

E-mail: Harold.Yepes@ific.uv.es

ABSTRACT: ANTARES is actually the fully operational and the largest neutrino telescope in the Northern hemisphere. Located in the Mediterranean Sea, it consists of a 3D array of 885 photomultiplier tubes (PMTs) arranged in 12 detection lines (25 storeys each), able to detect the Cherenkov light induced by upgoing relativistic muons produced in the interaction of high energy cosmic neutrinos with the detector surroundings. Among its physics goals, the search for neutrino astrophysical sources and the indirect detection of dark matter particles coming from the sun are of particular interest. To reach these goals, good accuracy in track reconstruction is mandatory, so several calibration systems for timing and positioning have been developed.

In this contribution we will present the design of the detector, calibration systems, associated equipment and its performance on track reconstruction.

KEYWORDS: Large detector-systems performance; Performance of High Energy Physics Detectors; Detector alignment and calibration methods (lasers, sources, particle-beams)

© 2012 IOP Publishing Ltd and SISSA

doi:10.1088/1748-0221/7/01/C01022

Contents

1 Introduction **1**

2 The ANTARES instrumentation **1**
2.1 Main components 1
2.2 Electronics design and performance 2
2.2.1 Data acquisition and signal processing 2
2.2.2 Amplitude calibration 4
2.3 Calibration systems 5
2.3.1 Timing calibration 5
2.3.2 Positioning determination 6

3 Detector performance: track reconstruction **7**

2012 JINST 7 C01022

1 Introduction

High energy neutrino astronomy aims to detect cosmic neutrinos which arrive at the Earth from the deepest regions of the universe. Due to neutrino features, neutrino observation requires large volume and massive detector systems. Astroparticle physics at GeV/PeV energy range, as well as particle physics and earth sciences can be studied. The ANTARES operation over 5 years since the installation of its first detection line has met expectations showing reliability of neutrino astronomy in the Mediterranean Sea, from its front-end electronics performance to the viability of its main physics program. Key aspects in the ANTARES detector achievement will be described in the following sections.

2 The ANTARES instrumentation

2.1 Main components

The ANTARES detector is a 3D grid of 12 detection lines with 25 storeys per line where detection units called Optical Modules (OM) are coupled in triplets. The OM is a high pressure resistant glass sphere housing a 10” Hamamatsu PMT (14 dynodes), and using a μ-metal cage as shield from Earth’s magnetic field. Consecutive storeys are separated by 15m and the distance between adjacent lines by 60m. A storey is basically equipped with triplet of PMTs for light collection, the electronics container and a set of light/sound devices for calibration. The transit time (TT) of the PMT is monitored by an internal LED [1]. The Local Control Module (LCM) is a titanium container which houses all the electronics of the storey. Among its main devices there are the Local Power Box (LPB), the clock board (CLK), the DAQ/Slow-Control board, the compass mother board and the Analogue Ring Samplers (ARS) motherboards as well as a system for analogue

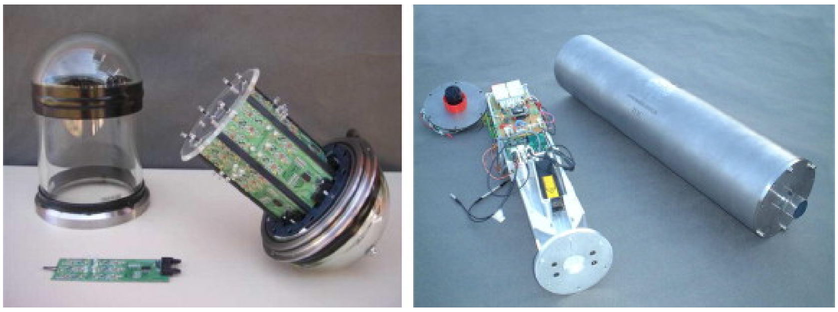

Figure 1. Optical Beacon System. Left: LED OB. Right: Laser OB.

signal processing and digitization. Each five storeys (a sector) a LCM (MLCM) is equipped with some extra devices for signals multiplexing, communication and electrical-optical conversion by means of a Dense Wavelength Division Multiplexing (DWDM-MB) and a BIDICON mother board respectively. An Ethernet SWITCH connects the processor of the MLCM-BIDICON card via the backplane [1].

The light sources are known as the Optical Beacon (OB) System [2]. There are two kind of them: the LED OB (LOB) and the laser OB. The LOB is a hexagonal frame composed by six blue LEDs (470 nm) per face which flashes light with a well known emission time. There are four LOB strategically placed along the lines for inter-storey time calibration [3]. Moreover they can be used for monitoring optical properties of the water [4] (two modified OBs are also used with multi-wavelength LEDs). The read-out signal of the LOB is done by an internal PMT and a variable capacitor allows the synchronization of the emission time of the 36 LEDs disposed over the LOB faces. The Laser OB is a diode pumped Q-switched Nd-YAG laser (532 nm) which produces very short light pulses, it can operate at variable light intensity by means of a crystal liquid attenuator system working jointly with a crystal rod and a diffuser. There are two Laser OB at the bottom of two central lines mainly used for inter-line time calibration as well as for positioning and for monitoring optical properties of the water. An internal fast photodiode identifies the emission time of the Laser light pulse. The OB system can be seen in figure 1.

The sound devices installed in the storey are basically 5 hydrophones (sound receivers) located along the line which by means of a triangulation basis with some autonomous transponders at the bottom of the lines, detect sound waves with particular features making possible the positioning of the OMs. Finally, at the bottom of each line is installed the String Control Module (SCM), which collects the data stream from the line and send to shore by means of the Main Electro-Optical Cable (MEOC) connected to the Junction Box (JB) where the detector lines converge.

2.2 Electronics design and performance

2.2.1 Data acquisition and signal processing

The data acquisition (DAQ) in ANTARES is based on the “all-data-to-shore” concept. The signals of each PMT are digitized *in-situ* by two ARS working in a token ring configuration in order to decrease the electronics dead time. The ARS can enable two modes of operation: single-photoelectron (SPE) signals and multi-form waveform (WF) signals [5], where an analogue Pulse

2012 JINST 7 C01022

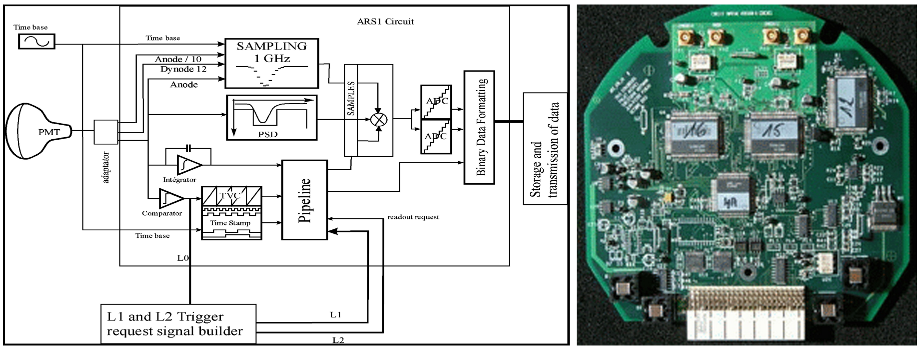

Figure 2. Left: ARS architecture. Right: ARSs in MB: 15-16 for signal processing; 12 for trigger duties.

Shape Discriminator (PSD) performs the selection. SPE signals are compatible signals in time width and amplitude with the single-photoelectron profile. Figure 2 shows the ARS architecture.

The ARS circuit design includes 24 Digital-to-Analogue Converters (DAC) (3–8 bits), 2 Analogue-to-Digital Converters (ADC) (8-bit), integrator + 8-bit Amplitude-to-Voltage-Converter (AVC), a 8-bit Time-to-Voltage-Converter (TVC), a 16-memory-cell pipeline (data storing, 16 SPE hits or 4 WF hits) and an 128-cell deep analogue sampler (4 channels) for signal sampling up to 1 GHz. The sampler in the ARS chips has four inputs where the PMT anode signal, the master clock signal (20 MHz), the PMT attenuated signal and the signal of the PMT 12-dynode are connected. In the SPE mode the digitization of the signal is carried out when the electrical signal exceeds a low threshold of 1/3 of the single photo-electron (PE) average amplitude (L0 level $\sim$ 0.3 PE), if the SPE profile matches, the signal is time-stamped (TS) with the master clock signal and the TVC and integrated by the AVC in a 35 ns time window [5]. In the WF mode the PMT signal is recorded in detail since it is sampled together with the clock signal by means of a set of 128 switched capacitors running between 0.15 and 1 GHz, for a sampling of 128 times every 1.6 ns. This mode is mainly used for calibration and detector tuning purposes and its good resolution lets to distinguish between two concecutive pulses [5], however due to the amount of data collected in WF mode, only SPE signals are currently recorded for physics analysis in ANTARES.

The time information is recorded by the TVC when a ramp generator furnishes a voltage proportional to the time within two subsequent clock pulses ($\sim$ 50 ns). When the signal reaches the L0 level the ramp voltage is memorized with its TVC value. Since the fall back to the base voltage is not instant, a flip-flop scheme based on two TVC ramps is used [5].

The charge measurement by the AVC is done in several steps (to minimize charge losses) by means of three switched capacitors: integration (signal from the anode is integrated), memorization (integrated charge is recorded in the pipeline memory) and charge erasing (pipeline memory is reset) [5]. Such phases are carried out in a cycle of period between 8–30 ns (longer than the PMT rise time $\sim$ 8 ns). Once L0 level is reached, the time integration is increased in order to surround all the signal pulse shape (between 17–50 ns). The integrated charge is the result of the addition of the collected charge in the two capacitors in the integration and memorization phase. After integration, the charge is digitized by the AVC and the PSD returns a binary result if the pulse is SPE or WF type, afterwards the data is stored with their corresponding AVC-TVC, TS-PSD respectively.

The "all-data-to-shore" scheme implies that all signals exceeding the L0 level are digitized,

2012 JINST 7 C01022

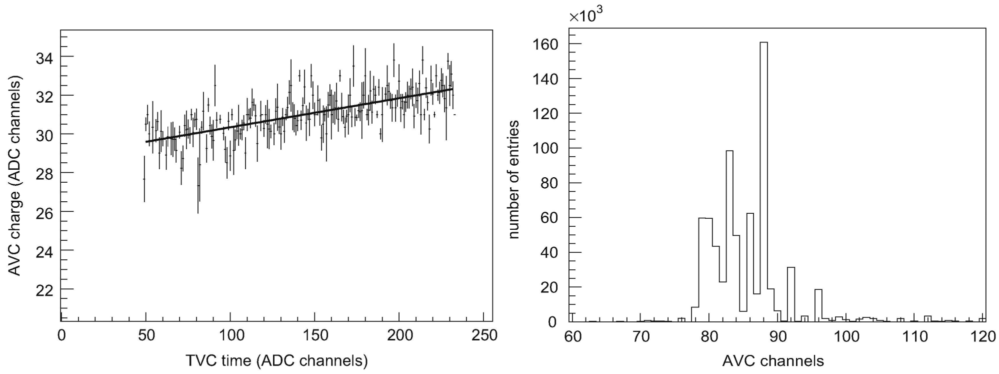

Figure 3. Left: cross-talk effect on charge measurements. Right: a typical AVC distribution

sent to shore (700 Mb/s per line) and processed in real time by a farm of PCs. Due to the large amount of data, several levels of multiplexing are required. The first level is carried out into the LCM of each storey where a Field Programmable Gate Array (FPGA) and the microprocessor in the DAQ card outputs the digitized data of the three OMs. In the second level, the MLCM of a sector gathers the data from the local OMs and from the other four connected storeys by means of an Ethernet SWITCH, and sends the data stream to the third multiplexing level through the DWDM which is performed at the bottom of the line at the SCM. Here, multiplexers and de-multiplexers pack the data of the line and sent to shore via the MEOC connected to the JB. The last level is the de-multiplexing level in the shore station where the data are processed and filtered by a PC farm and sent by optical fibre to the computer center to be stored and made available for analysis. Finally, an on-line trigger selects events according to the physics under study (muon events, OB events, etc.).

2.2.2 Amplitude calibration

The amplitude calibration relies on the measurement of the corresponding photo-electron peak and the pedestal value of the AVC channel. The procedure involves the read-out of the output signal of the PMT during special data taking sessions recording the optical activity in the sea due to ^{40}K decays and bioluminescence bacteria which produce primarily single photons at the photocathode level [5]. Some ARS design features have to be considered towards the expected electronics achievement: cross-talk effect, DNLs effect and walk effect.

The charge measurements in the ARS are affected by a "cross-talk" effect due to the influence of the TVC ramp values on the analogue memory of the AVC during the ARS signal digitization. However, TVC values are not affected by the AVC digitization. The cross-talk correction (up to 0.2 photo-electrons) is performed on a event-by-event basis plotting AVC-TVC as figure 3 left shows.

Non-uniform bin sizes or "Diferential Non-Linearities (DNL)" are seen as empty channels in AVC distributions as figure 3 right shows. A way to reduce this effect is to treat the TVC and AVC distributions as cumulative distributions.

The "walk effect" occurs when two signals coincident in time at their maximum with different amplitudes exceed the L0 level at different times, which gives a photon time delay as function of the charge. This effect is parameterized from the amplitude as function of the hit time.

2012 JINST 7 C01022

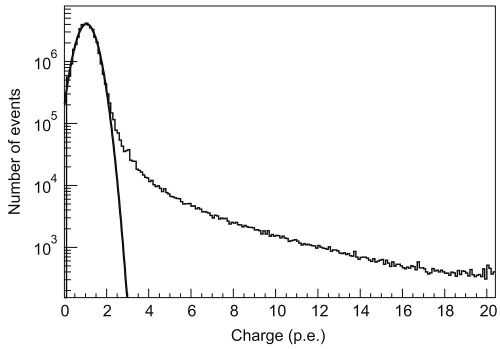

Figure 4. Calibrated charge distribution for all PMTs in the detector.

Once these effects have been corrected, all hits which exceed the L0 level are parameterized in charge distribution according to the next equation:

$$dN/dx = Ae^{-\alpha(x-x_{th})} + Be^{-(x-x_{pe})^2/2\sigma^2} \tag{2.1}$$

where x is the charge, x_{th} the effective threshold and x_{pe} the photo-electron peak, all of them in ADC units. The dark current of the PMT and the photo-electron distribution approach are taking into account on the first and second term respectively in 2.1. The charge calibration is applied to reconstruct the amplitude of the individual signals from the OMs. In this sense, the distribution is peaked at one photo-electron as it is expected for the optical activity signals as can be seen in figure 4.

The linear response integrator-ADC provides the equivalence of ADC counts into photo-electron units as the difference between the one photo-electron peak and the pedestal value of the AVC:

$$Q_{pe} = \frac{AVC - AVC_0}{AVC_1 - AVC_0} \tag{2.2}$$

where AVC_0 and AVC_1 are the values which match to the pedestal and the photo-electron peaks respectively.

2.3 Calibration systems

2.3.1 Timing calibration

The time calibration in ANTARES is performed before and after the immersion of lines in the sea. Before immersion several tests are carried out with a dedicated calibration set up in a *dark-room* in order to estimate the time offsets between detection units, by means of Laser, clock and LEDs in the OM. Once at the site the relevant constants measured on-shore are re-computed since they could change slightly due to temperature changes, stretching of cables due to transport/deployment activities, and also when high voltages applied to the PMTs are tuned [3]; this is carried out by the OB system mentioned in section 2.1 and cross-checked by alternative methods, such as coincidence analysis of ^{40}K decays and time residuals computed from down-going muon tracks. The time calibration relies on an absolute and a relative determination. The absolute time calibration refers to the assignment of a universal time for each event and this is achieved by interfacing the shore station masterclock with a card receiving the Global Positioning System (GPS) time ($\sim$ 100 ms

2012 JINST 7 C01022

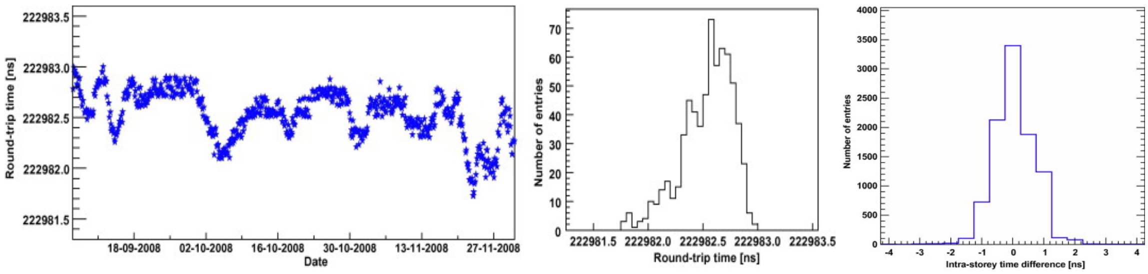

Figure 5. Left-Center: Round-trip time on-shore - SCM. Right: Time differences for a pair of OMs.

accuracy respect to the Universal Time Coordinated (UTC)) on the LCM. The main uncertainty for the absolute time calibration comes from the electronics path common to all OMs. This is measured by a common synchronization signal to estimate the round-trip time from shore to each SCM. The time to correlate detector events (∼1 ms is precise enough) with astrophysical phenomena is reached at nanosecond level by the master clock system and its time stability is maintained as figure 5 (center, left) shows:

The relative time resolution concerns the time offsets between detection units. Several factors, such as the transit time spread (TTS) of the PMT, the light propagation, electronics from the light source and the acquisition system, impact on the time resolution of the detection units as follows:

$$\sigma^2_{OM} = \frac{\sigma^2_{TTS}(\sim 1.3ns)}{N_{pe}} + \frac{\sigma^2_{water}(\sim 1.5ns)}{N_\gamma} + \sigma^2_{OB} + \sigma^2_{elec} \tag{2.3}$$

To reduce the TTS and the light propagation contribution, the time offset computation is performed with the closest OMs to the OB in order to increase the number of photons collected by the PMT (N_{pe}) and reaching the OM (N_γ), reducing in this way the contribution of the first two terms in 2.3. The contribution of the third term is negligible due to the fast OB internal PMT rise time. Therefore, the main contribution comes from the electronics and a resolution ∼0.5 ns ($\sigma/\sqrt{2}$) is reached as can be seen in figure 5 (right), enough to achieve an angular resolution (angle between real and reconstructed track) in the detector less than 0.5° for E_ν>10 TeV.

2.3.2 Positioning determination

An accurate positioning of all the OMs is needed to have the expected detector performance. The ANTARES acoustic positioning system includes 1 transceiver/receiver (T_x/R_x) at the bottom of the lines and 5 hydrophones (R_x) per line at specific heights, plus a set of compasses and velocimeters, one per storey [1]. The measurements are performed every two minutes by means of autonomous transponders for triangulation which emit acoustic sinusoidal wave packets of 2 ms duration with frequency ∼40–60 Hz as signal identity. Compasses give the heading and the tilt. For the reconstruction of the line shape a global χ^2 fit is performed to a model based on the mechanical behaviour of the line (weights and drag coefficients) due to sea water flow. This mechanical model provides the radial displacement as function of the vertical coordinate z:

$$r(z) = [az - bLn(1 - cz)]v^2 \tag{2.4}$$

where a, b, c are known mechanical constants and v is the sea current velocity which is left as a free parameter. This system has provided a precision of 10 cm [1].

2012 JINST 7 C01022

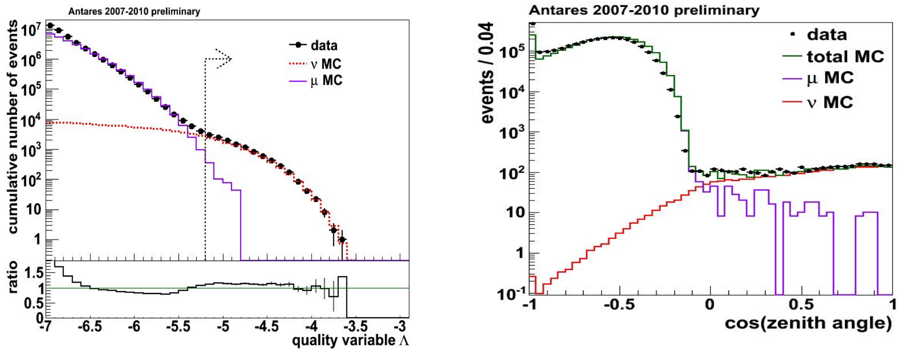

Figure 6. Left: Reconstruction quality variable distribution. Right: Zenith angle distribution for tracks.

3 Detector performance: track reconstruction

The standard muon trigger aims for a hit selection due to Cherenkov photons by rejecting the optical background or Cherenkov scattered hits based on the arrival time of the hits, the distance between PMTs and the speed of light, without any assumption on the track direction since sensitivity to the full sky is expected [6]. In order to avoid constraints because rates of accidental correlations an increase of purity of event samples is mandatory and the pre-selection of the sample requires additional trigger levels after L0 level. The L1 level is achieved when a high threshold of $\sim$2.5 PE is exceeded or a coincidence of at least two L0 levels from different OMs is founded inside a 20 ns time window on the same storey. The L2 level requires the fulfillment of L0 and L1 criteria. More refined triggers as the T3 trigger which seek for a coincidence of two L1 in 80 or 160 ns time window can be defined also.

Once tha data is stored on-shore, some offline algorithms based on the likelihood maximization of the hit times as function of the muon direction can be applied. Typically for muons, a coincidence < 20 ns on a storey (L1 level) and at least 5 L1 in coincidence gives a physics event. The physics events are treated with a multi-stage fitting procedure [6]. The first stages perform the hits selection and set up the starting point for the final fit. In the final stage the fit of the likelihood to the observed hit times including the contribution of the optical background is made taking into account several starting points to increase the probability to find the global likelihood maximum. A quality variable (Λ) for the reconstructed track is defined as function of the maximum likelihood. figure 6 (left) shows the cumulative distribution of the quality variable Λ, well reconstructed tracks are defined for $\Lambda > -5.2$. Figure 6 (right) shows the distribution of the cosine of the zenith angle of the tracks, both for data and Monte Carlo. The agreement is rather good and more than 3000 up-going tracks (cos[zenith] > 0) have been well reconstructed and selected for dedicated physics analysis.

Acknowledgments

We gratefully acknowledge the support of Spanish Ministerio de Ciencia e Innovación (MICINN), grants FPU AP2008-00775, FPA2009-13983-C02-01, ACI2009-1020, MultiDark Consolider CSD2009-00064 and of the Generalitat Valenciana Prometeo/2009/026.

2012 JINST 7 C01022

References

[1] M. Ageron et al., *ANTARES: the first undersea neutrino telescope*, *Nucl. Instrum. Meth.* **A 656** (2011) 11 [arXiv:1104.1607].

[2] ANTARES collaboration, M. Ageron et al., *The ANTARES Optical Beacon System*, *Nucl. Instrum. Meth.* **A 578** (2007) 498 [astro-ph/0703355].

[3] THE ANTARES collaboration, J. Aguilar et al., *Time Calibration of the ANTARES Neutrino Telescope*, *Astropart. Phys.* **34** (2011) 539 [arXiv:1012.2204].

[4] H. Yepes-Ramírez, *Water absorption length measurement with the ANTARES optical beacon system*, *Nucl. Instrum. Meth.* **A 626-627** (2011) S118.

[5] J.A. Aguilar et al., *Performance of the front-end electronics of the ANTARES Neutrino Telescope*, *Nucl. Instrum. Meth.* **A 662** (2010) 59.

[6] S. Adrián-Martínez et al., *First search for point sources of high-energy cosmic neutrinos with the ANTARES neutrino telescope*, *Astrophys. J. Lett.* **743** (2011) L14.

2012 JINST 7 C01022